ACTIVE-FLUX BASED OBSERVER FOR MOTION SENSORLESS CONTROL OF BIAXIAL EXCITATION GENERATOR/MOTOR FOR AUTOMOBILES (BEGA)

V. COROBAN[*]

[*]*University "Politehnica" of Timisoara, Faculty of Electrical Engineering, Timisoara, Romania*

I. BOLDEA[*]**, G.-D. ANDREESCU**[**]

[**]*University "Politehnica" of Timisoara, Faculty of Computer Science Engineering, Timisoara, Romania*

Abstract*. This paper proposes an active flux observer for motion-sensorless biaxial excitation generator for automobiles (BEGA) for wide speed operation. The active flux observer transforms BEGA, a salient-pole rotor ac machine, in a virtually non-salient pole machine model so that the rotor speed and position can be estimated in a simpler way. Simulations and experimental results are presented to verify the principles and to demonstrate the performance of the proposed observer. A rotor position and speed estimator, based on active flux estimation is proposed and tested. The performance (accuracy) of the observers has been tested with the drive system operated from very low speed down to 2 rpm, with full load and up to 2000rpm.*

Key words: *active flux observer, vector control, unity power factor, dc excitation, current referencer.*

1. Introduction

BEGA is proposed as a solution for integrated starter-alternator system used in hybrid electric vehicles. This solution is a compromise between power, efficiency and cost. BEGA has a standard three-phase stator with uniform slots and a three-phase winding while in the rotor it has a heteropolar dc excitation winding (in d-axis) and a lower cost permanent magnets (PMs) located in the multiple flux-barriers (in q-axis). This mix between a standard permanent-assisted reluctance synchronous machine (PM-RSM) and dc excited synchronous machine is characterized by:

- Higher efficiency than conventional claw-pole alternator. The large claw-pole eddy-currents losses are eliminated. The large voltage and flux harmonics at high speeds are considerably low than in the claw-pole alternator
- The low-cost ferrite PMs placed in the multiple flux barriers are designed to "fully destroy" the q-axis stator-produced flux linkage. For PM-RSM the PMs flux interaction with i_d current give the main component of the torque; for BEGA the vector control (for i_d=0 and i_q=0) the torque is produced by interaction of dc excitation current field and i_q stator current.
- A 4-quandrant dc-dc converter is required to control the dc field current regulation. The rated power of the converter is approx. 5% of machine rated power.
- The stator current for the same torque is considerably lower (even 30%) than for the PM-RSM. This has a direct impact on the rated power of the three phase inverter.
- BEGA is capable of a very large constant power speed range (CPRS). Theoretically this ratio is infinite but due to mechanical limitation and losses a ratio of 10-20 is considered practical. Very large CPRS has been demonstrated by simulations and experiments with encoder feedback [4].

A cross-section of BEGA is given in Fig. 1.

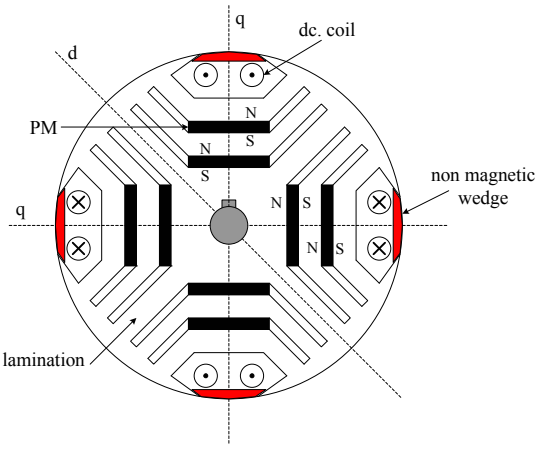

Fig.1 BEGA rotor cross-section

The prototype design and a comprehensive characterization with test results is presented in [1,2,3]. A vector control structure, with position and speed sensor for BEGA, is proposed and tested in [5,6]. This paper is focused on rotor position and speed estimation of BEGA, from the active flux observer, in an effort to reduce the on-line computation effort and to provide very low speed operation without any signal injection. The principles have been verified experimentally and have proven to work for very low speed operation.

2. BEGA – Mathematical model

The BEGA transient equations in d-q reference frame are:

$$\bar{v}_s = R_s \bar{i}_s + \frac{d\bar{\psi}_s}{dt} + j\omega_r \psi_s \tag{1}$$

$$\bar{v}_s = v_d + jv_q \;;\; \bar{i}_s = i_d + ji_q \;;\; \bar{\psi}_s = \psi_d + j\psi_q \tag{2}$$

$$\psi_d = L_d i_d + L_{mf} i_F \;;\; \psi_q = L_q i_q - \psi_{PM} \tag{3}$$

$$t_e = \frac{3}{2} p_1 \left(\psi_d i_q - \psi_d i_q\right) \tag{4}$$

$$v_F = R_f i_F + \frac{d\psi_F}{dt} \;;\; \psi_F = L_{mf} i_d + L_f i_F \tag{5}$$

where $\bar{v}_s$, $\bar{i}_s$ are the stator voltage and current vector respectively, is the stator flux linkage vector, R_s is the stator resistance, ω_r is the electrical rotor speed, are the d, q axis inductance, L_{mf} is the mutual field-armature inductance, ψ_{PM} is the PM flux on q axis, and p_1 is the pole pair. Equation (5) characterizes the dc field (excitation) circuit, where v_F, i_F is the field voltage and current respectively; ψ_{PM} is the field flux, and R_F are the field winding resistance and inductance, respectively. Equation (5) shows that during i_d current variation (transients) an overvoltage may occur in the dc field circuit. To avoid this overvoltage in the dc field circuit a simple protection made by a resistor and a static switch or a varistor is used.

During the unity power factor operation (with zero i_d and zero ψ_q), from (1)-(5), the steady-state dq equations of BEGA become:

$$v_s = R_s I_{qk} + \omega_r L_{mf} i_F \quad i_s = I_{qk} = const \tag{6}$$

$$t_e = \frac{3}{2} p L_{mf} i_F I_{qk} \;;\; \bar{i}_s = jI_{qk} \tag{7}$$

where $I_{qk}=\Psi_{PM}/L_q$. Implicit unity power factor operation is obtained. The machine operation can be switched from motoring to generating in two ways: a) by changing the sign of current, but in this case the machine does not operate at unity power factor b) by changing the sign dc. excitation current.

The vector diagram at unity power factor operation is illustrated in Fig. 2

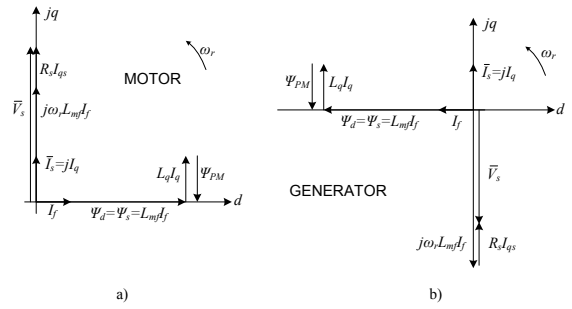

Fig.2 BEGA steady state vector diagram at unity power factor a) motoring mode b) generating mode

3. Active-flux concept for BEGA

The "active flux" concept proposed in [6] transforms all salient-pole rotor ac machines into virtually nonsalient-pole models, such that the rotor position and speed estimation becomes simpler.

For BEGA the active flux is expressed as:

$$\begin{aligned} &\bar{\psi}_d{}^a = \bar{\psi}_s - L_q \bar{i}_s = \\ &= L_{mf} i_f + L_d i_d + j\left(L_q i_q - \psi_{PMq}\right) - L_q \left(i_d + ji_q\right) \\ &\bar{\psi}_d{}^a = L_{mf} i_f - j\psi_{PMq} \;;\; \bar{i}_s = ji_q \quad for\ i_d = 0; \end{aligned} \tag{8}$$

The torque expression remains the same, as in eq. (3).

The steady state vector diagram of BEGA (for id=0), with in foreground, is drawn in Fig. 3.

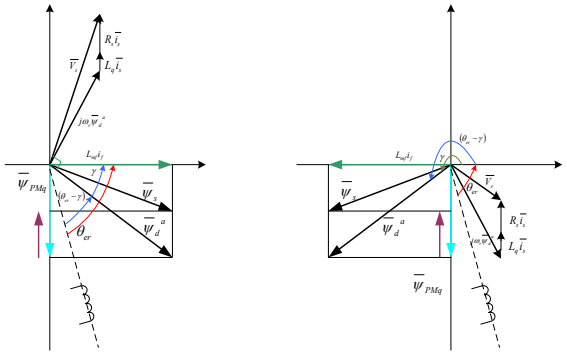

Fig.3 BEGA and its vector diagram pointing out the active flux , for a) motoring and b) generating

The stator voltage model of BEGA in stator coordinates is:

$$\bar{V}_s = R_s \bar{i}_s + \frac{d\bar{\psi}_s}{dt} \tag{9}$$

The stator voltage model, taking into account the active flux, becomes:

$$\bar{V}_s = R_s \bar{i}_s + (s + j\omega_r) L_q \bar{i}_s + (s + j\omega_r) \bar{\psi}_d{}^a \tag{10}$$

The vector diagram of eq. (10) is illustrated in Fig. 3.

The active flux observer, in stator coordinates, is:

$$\bar{\psi}_d{}^a = \int \left(\bar{V}_s - R_s \bar{i}_s + V_{comp}\right) - L_q \bar{i}_s \tag{11}$$

where:

$$\bar{\psi}_d{}^a = \psi_d{}^a \cos\left(\theta_{er} - \gamma\right) + \psi_d{}^a \sin\left(\theta_{er} - \gamma\right) \tag{12}$$

The compensation voltage vcomp deals with the inverter nonlinearities, integrator offset, and stator resistance variation. We have added (Fig. 6) a stator flux current model a PI regulator to accomplish robustness of the active flux observer over wide speed range.

4. Experimental platform

A set of experiments were carried out to prove the validity of the proposed solution (zero i_d and zero Ψ_q). The structure of experimental platform is shown in Fig. 4.

BEGA (Table 1) is fed through a 48Vdc, 350A Sauer-Danfoss three phase inverter from a 48V, 55Ah valve regulated lead-acid battery pack. The BEGA was mechanically coupled with a three phase induction machine (IM) via a transmission belt ($n_{IM}/n_{BEGA}=1/2$). The

IM was driven by an ABB ACS600 bidirectional converter. The rated power of IM was 5.5kW at n=2945 rpm, enough to load the BEGA at full load. A four quadrant dc-dc converter with $I_{dc\_rated}=5A$, $V_{dc\_rated}=48V$ was built for current control in the dc. field winding. An incremental encoder (Telemecanique XCC-1510PR50R, 5000ppr) was used for BEGA position and speed measurement.

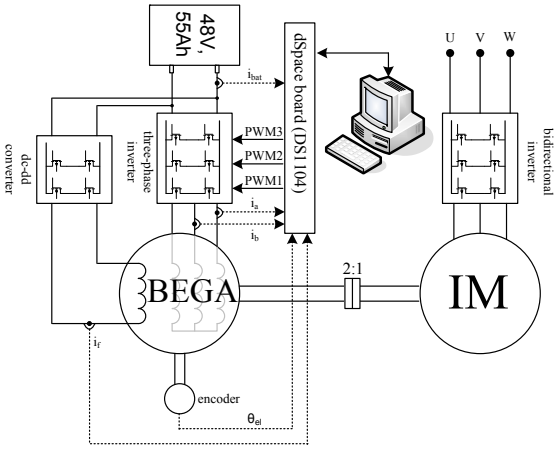

Fig.4 Experimental platform for BEGA control

The control algorithm has been developed in Matlab-Simulink and implemented on a dSpace 1104 Real Time System (RTI) used for rapid prototyping. The following signals were measured using dSpace acquisition board: phase currents, battery current, dc field current, phase voltages, battery voltage and BEGA rotor position.

Tab. 1. BEGA parameters

Rated power (P_N)	*2.35 kW*
Rated phase voltage (V_s)	*22 V (rms)*
Rated phase current (I_s)	*67 A (rms)*
Rated field current (I_f)	*5 A*
Rated battery voltage (V_{batt})	*48 V*
Rated torque (T_N)	*15 Nm*
Rated speed (n_N)	*1500 rpm*
Number of pole pairs (p)	*2*
Stator phase resistance (R_s)	*0.05 Ω*
q axis inductance (L_q)	*0.455 mH*
d axis inductance (L_d)	*1.8 mH*
PM flux (Ψ_{PM})	*0.0136 Wb*
Field winding resistance (R_f)	*6.5 Ω*
Field winding inductance (L_f)	*0.300 H*
Mutual field-armature inductance (L_{mf})	*16.5 mH*
Moment of inertia (J)	*16e-3 kg·m^2*
Viscous friction coefficient (B)	*1e-4*

5. Proposed bega sensorless vector control system

Fig. 5 illustrates the proposed speed sensorless control system for BEGA. The commanded input is the target rotor speed (Fig. 5). The current referencer provides the target current components on q-axis (i_q^*) and target dc field (i_F^*) while the reference d-axis current (i_d^*) is set to zero. The current referencer provides the reference current combination (i_q^*, i_F^*), that ensure minimum total copper losses in the machine. More details about the current referencer can be found in [4].

The relationship used for reference q-axis current (i_q^*) calculation is given by equation (13):

$$i_q = I_{qk}\sqrt{\frac{|t_e^*|}{|t_{ek}(\omega_r)|}} \tag{13}$$

where $I_{qk}=\psi_{PM}/L_q$, is the q-axis current that ensures cancellation of the total q-axis flux ($\psi_q=0$). For $i_q=I_{qk}$ and $i_d=0$ unity power factor operation of BEGA is guaranteed and the ratio torque/ampere is maximized.

Equation (14) calculates the d-axis flux component given by dc field current which, in combination with the current given by eq. (13), develops the requested torque, provided by speed controller.

$$\psi_F^* = \frac{2\cdot t_e^*}{3\cdot i_q^*\cdot p_1} \tag{14}$$

From the non-linear magnetization curve, stored in a look-up table, the reference dc field current (i_F^*) is extracted.

The current controllers are implemented in rotor reference frame and produce the reference stator voltage. The d-axis controller should not be calibrated for a very fast response, in order to avoid induced voltage in the dc field excitation due to fast id transients. The space vector modulation has as main inputs the stator voltage reference (V_α^*, V_β^*), and it gives the switching command signals (T1..6) for the voltage source inverter. For the coordinates transformation the measured electrical rotor position is used, which is furthermore used as a basis for the evaluation of the position observer performance. Also, the measured rotor speed is used in vector control structure. So the drive is encoder control and the investigation focuses on the quality of the flux, position and speed estimation.

6. State observers

6.1. The active flux observer

The observer task is to estimate the active flux in a wide speed range.

The operating principle of the proposed observer is to extract the active flux using the measured stator current, dc. field current and the estimated stator voltage. The stator voltage is estimated based on the measured dc-link (battery) voltage and the switching states.

The signal flow diagram of active flux observer is shown in Fig. 6. It is based on a combined voltage-current model from which the $L_q i_s$ term is subtracted.

The stator flux observer combines advantages of the current-model estimator in rotor reference at low speed, with the voltage-model estimator in stator reference at medium high speed, using a dynamic compensation (PI compensator).

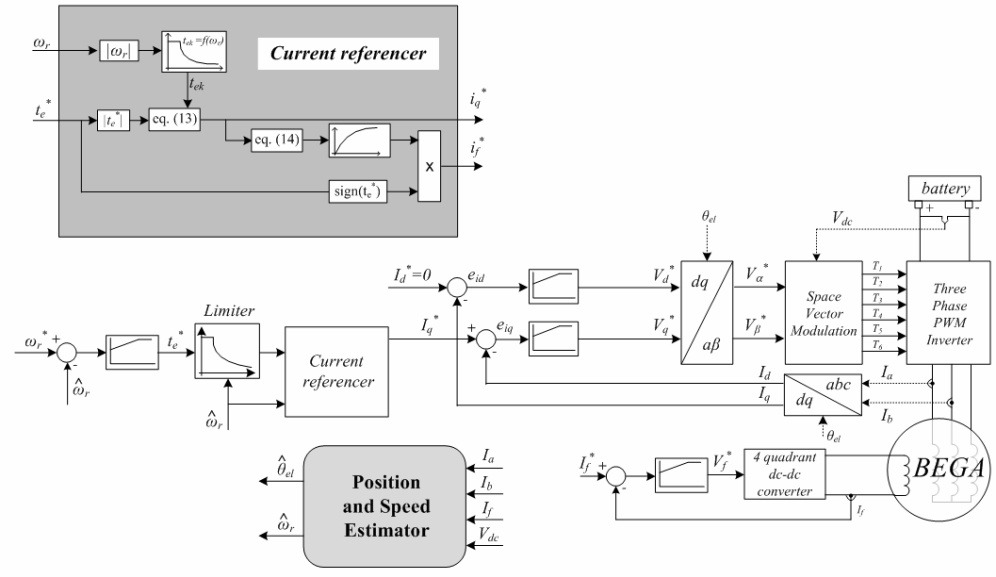

Fig. 5. BEGA Vector Control Structure

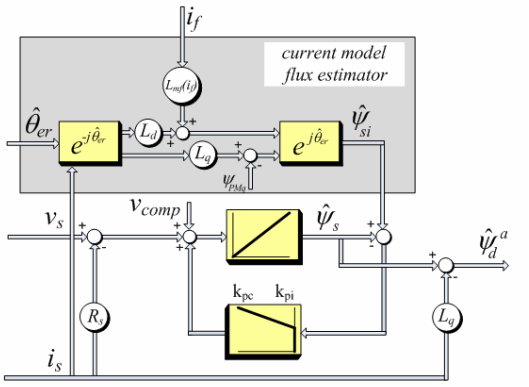

Fig. 6. Active flux observer in stator reference frane

The values of k_{pc} and k_{ic} decide the speed range where the current model (or voltage model) prevails.

$$x = \left(k_{pc} + \frac{k_{ic}}{s} \right) \left(\hat{\psi}_{si} - \hat{\psi}_s \right) \tag{15}$$

where and are the stator flux estimated based on current model and respectively voltage model.
The PI compensator parameters k_{pc} and k_{ic} are defined as:

$$k_{pc} = \omega_1 + \omega_2 \quad ; \quad k_{ic} = \omega_1 \cdot \omega_2 \tag{16}$$

where $[0...\omega_1]$ is the speed range where the current model based stator flux estimator prevails and $[\omega_2...\omega_{max}]$ is the speed range where the voltage model stator flux estimator prevails. Also, the PI compensator rejects the dc offset and drifts from the current acquisition [2].

The vcomp term is used only to compensate the voltage drop on the inverter MOSFETs (inverter non-linearities). It is expresses as follows:

$$v_{comp(a,b,c)} = R_{ds\_on} \cdot i_{(a,b,c)} + v_{th} \tag{17}$$

where R_{ds_on} is drain-source resistance of the MOSFET during conduction and vth is the threshold voltage of the MOSFET.

This compensation is proposed in [7] in a different form but the results are equivalent.

6.2. Position and speed estimator

The rotor position and speed estimator implementation is presented in Fig. 7. To extract the rotor position and speed from the active flux vector, a PLL (phase-locked-loop) state-observer is employed. The output of the PLL is the estimated position of the active flux ($\hat{\theta}_{er} - \gamma$). To obtain the estimated position of the rotor, the angle γ is added to the estimated position of active flux.

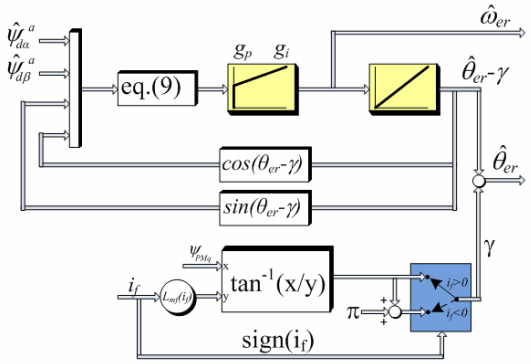

Fig. 7. Rotor position and speed estimator

$$x = -\hat{\psi}_{d\alpha}{}^{a} \sin\left(\hat{\theta}_{er} - \gamma\right) + \hat{\psi}_{d\beta}{}^{a} \cos\left(\hat{\theta}_{er} - \gamma\right) \tag{18}$$

The angle γ can be very precisely estimated due to accurate knowledge of and obtained from experiments.

$$\gamma = \begin{cases} \tan^{-1}\left(\psi_{PMq} / L_{mf} i_F\right) & , \text{ for } i_F > 0 \\ \tan^{-1}\left(\psi_{PMq} / L_{mf} i_F\right) + \pi & , \text{ for } i_F < 0 \end{cases} \tag{19}$$

The electrical rotor speed can be estimated from the rotor electrical position using equation (20):

$$\hat{\omega}_{er} = \frac{d\hat{\theta}_{er}}{dt} = \frac{d\left(\left(\hat{\theta}_{er} - \gamma\right) + \gamma\right)}{dt} \tag{20}$$

According to equation (20) the rotor electrical speed is expressed as a sum of two components: i) active flux speed and ii) gamma speed.

The active flux speed estimation is based on derivatives of active flux components ($\hat{\psi}_{d\alpha}{}^{a}$, $\hat{\psi}_{d\beta}{}^{a}$) as follow:

$$\hat{\omega}_r = \frac{\frac{d\hat{\psi}_{d\beta}{}^{a}}{dt}\hat{\psi}_{d\alpha}{}^{a} - \frac{d\hat{\psi}_{d\alpha}{}^{a}}{dt}\hat{\psi}_{d\beta}{}^{a}}{\left(\hat{\psi}_{d}{}^{a}\right)^2} \qquad (21)$$

$$\left(\hat{\psi}_{d}{}^{a}\right)^2 = \left(\hat{\psi}_{d\alpha}{}^{a}\right)^2 + \left(\hat{\psi}_{d\beta}{}^{a}\right)^2$$

A second solution for the speed estimation is given by equation (20):

$$\hat{\omega}_r = \frac{\frac{d\sin(\theta_{er})}{dt}\cos(\theta_{er}) - \frac{d\cos(\theta_{er})}{dt}\sin(\theta_{er})}{\left|\sin^2(\theta_{er}) + \cos^2(\theta_{er})\right|} = \qquad (22)$$

$$= \frac{\frac{\sin(\theta_{er})_{|t+\Delta t} - \sin(\theta_{er})_{|t}}{\Delta t}\cos(\theta_{er})_{|t} - \frac{\cos(\theta_{er})_{|t+\Delta t} - \cos(\theta_{er})_{|t}}{\Delta t}\sin(\theta_{er})_{|t}}{\left|\sin^2(\theta_{er})_{|t} + \cos^2(\theta_{er})_{|t}\right|}$$

where Δt is the sampling time of rotor speed evaluation.

The derivative estimation (21) gives very fast estimation of speed. The drawback of this solution is that the speed estimation accuracy is strictly dependent on the accuracy of the active flux components estimation. The accuracy of active flux depends on the electromagnetic parameters and the noise and offset of the measured signals. To remove the noise from the estimated speed a first-order low pass filter is used.

$$\hat{\omega}_{er}(k) = K \cdot \left(\hat{\omega}_{er}(k) - \hat{\omega}_{er}(k-1)\right) + \hat{\omega}_{er}(k-1) \qquad (23)$$

For the final approach the last solution was used due to lower noise in speed estimation. In fact the dc field derivative produces an unacceptable noise level which requires a strong low-pass filtering wihich furthermore gives a higher delay in the estimated speed.

7. Experimental and simulation results

A set of experiments were carried out for evaluation of the observers. The rotor speed during experiments was set to 2000, 200, 20 and 2rpm with motor loaded and unloaded. A large speed range is covered with these speed values. Due to limited space, only for extreme cases (2rpm, 2000rpm) the results will be presented.

The performance of the position and speed estimators in the high speed range is tested for a speed of 2000rpm. The experimental results are plotted in Fig. 8. The motor is accelerated from standstill to 2000rpm and then a few speed reversals take place. This way the convergence of the estimated rotor position during startup, transient and steady-state performance of the estimators can be analysed. The speed error during startup and transients slightly exceeds 50rpm, while at steady state is around 10rpm (error less than 0.5%). Less than 30ms are necessary for the position to converge to an error less than 30° (0.5rad electrical).

During speed reversal the maximum position error is below 12° electrical, while at steady-state the average position error is lower than 3°.

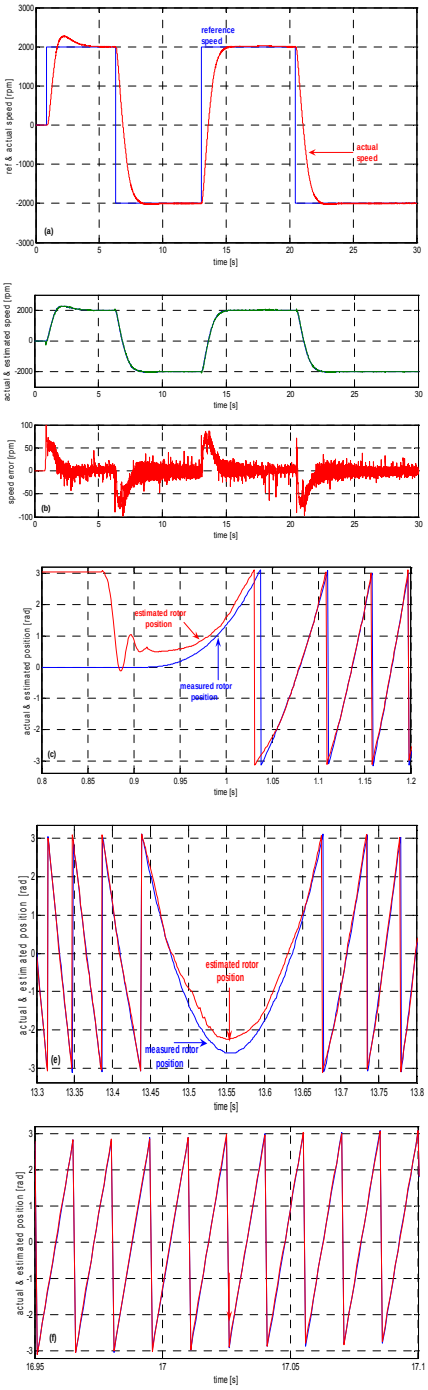

Fig.8 Experimental results: startup with load, ±2000 rpm speed reversal with load. From top to bottom: (a) reference and actual rotor speed, (b) zoom in on actual and estimated rotor position at startup, (c) zoom on actual and estimated rotor position at speed reversal (d) zoom on actual and estimated rotor position during steady-state (e) angle gamma (γ)

The γ angle has values closer to zero for motoring, while for generation the angle moves around 180°. The γ angle is giving us information about how much the BEGA is loaded. The closer γ to 0°, the higher the load for motoring and the closer γ to 180°, the higher the load for generating.

The performance of the observer and estimators at very low speed from zero to 2rpm and speed reversal at 2rpm, under no-load, are presented in Fig. 9.

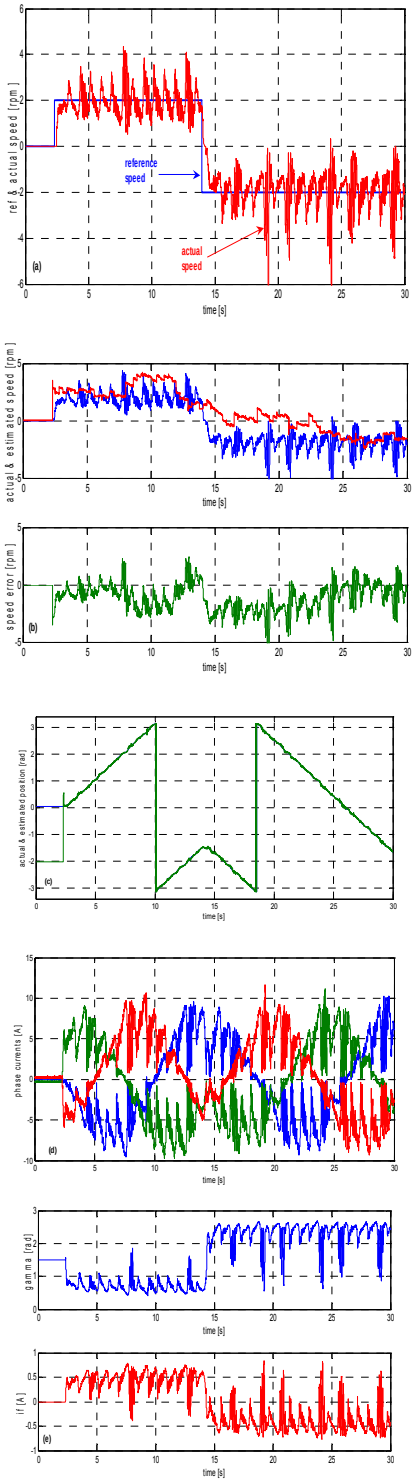

Fig.9 Experimental results: startup with load, ±2 rpm speed reversal with load. From top to bottom: (a) reference and actual rotor speed, (b) zoom in on actual and estimated rotor position at startup, (c) zoom on actual and estimated rotor position at speed reversal (d) zoom on actual and estimated rotor position during steady-state (e) angle gamma (γ)

The phase currents and dc field current are strongly distorted due to the high pulsations of cogging torque. The higher the magnitude of dc field current the higher the cogging torque magnitude. At zero dc field current ($i_F=0$) cogging torque is insignificant.

Therefore high nonlinear cogging torque will produce highly distorted currents at very low constant speed. Even with such distortions the accuracy of the estimated position is very good (around one electrical degree).

The explanation for such a good position estimation with such distorted currents is that all phase currents distortions (reflected in active flux observer) are counterbalanced by the dc field current distortion. This demonstrates the suitability of the active flux observer for BEGA position and speed estimation. The currents distortion decreases as the load increases due to the fact that cogging torque will become a smaller percentage of the total load torque. Good experiments under full load are possible only with a passive load or with a drive that is running with motion-sensor. Experiments under load were tried using as load a sensorless induction machine drive but the experiments failed. The corresponding speed of the loaded drive was 1rpm to the 2rpm of BEGA. Two electric machines running sensorless at such a low speed, one being use as a load is rarely.

8. Conclusion

An accurate rotor position and speed estimator based on the active flux observer for a wide speed range (2rpm to 2000rpm) is proposed and validated. Remarkable is the position accuracy of the position at very low speed. The speed estimation errors are acceptable during transients while at steady state they are below 1% (of rated speed) for higher speeds. Full motion sensorless control of BEGA experiments are under way with publication due soon.

References

[1] I. Boldea, S. Scridon, L. Tutelea, *"BEGA-a biaxial excitation generator for automobiles"*, Record of OPTIM-2000, Poiana Brasov, Romania.

[2] S. Scridon, I. Boldea, L. Tutelea, F. Blaabjerg, E. Ritchie, *"BEGA: Comprehensive characterization and test results "*, Record of IEEE-IAS-2004, Seattle, USA

[3] S. Scridon, I. Boldea, L. Tutelea, F. Blaajberg, A. E. Ritchie, *"BEGA – A Biaxial Excitation Generator for Automobiles: Comprehensive Characterization and Test Results"*, IEEE Trans. Vol. IA-41, no. 4, 2005, pp. 935-945

[4] V. Coroban, I. Boldea, G. D. Andreescu, F. Blaajberg, *"BEGA – Motor/Generator Vector Control for Wide Constant Power Speed Range"*, Record of OPTIM2006, Brasov, Romania

[5] I. Boldea, V. Coroban, G. D. Andreescu, S. Scridon, F. Blaabjerg, *"BEGA Starter/Alternator – Vector Control Implementation and Performance for Wide Speed Range at Unity Power Factor Operation "*, Record of IEEE-IAS-2008, Edmonton, Canada

[6] I. Boldea, M. C. Paicu, G. D. Andreescu, *"Active flux concept for motion sensorless unified ac drives"*, IEEE Trans. Power Electron., (to be published)

[7] P. L. Jansen, R. D. Lorenz, *"A physically insightful approach to the design and accuracy assessment of the flux observers for field orientation induction machine drives"*, IEEE Trans. Ind. Appl., vol. 30, no. 1, pp. 101-110, Jan./Feb., 1994

[8] J. Holz, J. Quan, "Drift and parameter compensated flux estimator for persistent zero stator frequency operation of sensorless controlled induction motors", IEEE Trans. Ind. Appl., vol. 39, no. 4, pp. 1052-1060. July/Aug. 2003